

VLBI Detection of an Active Radio Source Potentially Driving 100-kpc Scale Emission in the Ultraluminous Infrared Galaxy IRAS F01004–2237

TAKAYUKI J. HAYASHI ^{1,2} YOSHIKI HAGIWARA ³ AND MASATOSHI IMANISHI ^{1,3,4}

¹*National Astronomical Observatory of Japan
2-21-1 Osawa, Mitaka
Tokyo 181-8588, Japan*

²*Azabu Junior and Senior High School
2-3-29 Motoazabu, Minato
Tokyo 106-0046, Japan*

³*Toyo University
5-28-20 Hakusan, Bunkyo
Tokyo 112-8606, Japan*

⁴*Department of Astronomy, School of Science, Graduate University for Advanced Studies (SOKENDAI)
2-21-1 Osawa, Mitaka
Tokyo 181-8588, Japan*

Submitted to Astrophysical Journal

ABSTRACT

The nearby ultraluminous infrared galaxy (ULIRG) IRAS F01004–2237 exhibits 100-kpc scale continuum emission at radio wavelengths. The absence of extended X-ray emission in IRAS F01004–2237 has suggested an active galactic nucleus (AGN) origin for the extended radio emission, whose properties and role in merging systems still need to be better understood. We present the results of multi-frequency observations of IRAS F01004–2237 conducted by the Very Long Baseline Array at 2.3 and 8.4 GHz. Compact 8.4-GHz continuum emission was detected on a 1-pc scale in the nuclear region with an intrinsic brightness temperature of $10^{8.1}$ K suggesting that the radio source is originated from an AGN, potentially driving the extended emission. In contrast, no significant emission was observed at 2.3 GHz, indicating the presence of low-frequency absorption. This absorption cannot be attributed solely to synchrotron self-absorption; alternatively, free-free absorption due to thermal plasma is mainly at work in the spectrum. From combined perspectives, including mid-infrared and X-ray data, the AGN is obscured in a dense environment. The kinetic power of the nonthermal jet, as inferred from the extended emission, can play a more important role in dispersing the surrounding medium than the thermal outflow in IRAS F01004–2237. These findings hint that jet activities in ULIRGs may contribute to AGN feedback during galaxy evolution induced by merger events.

Keywords: Ultraluminous infrared galaxies (1735) — Radio continuum emission (1340) — Active galactic nuclei (16) — Very long baseline interferometry (1769)

1. INTRODUCTION

Galaxies with large infrared luminosity greater than $10^{12}L_{\odot}$ are known as ultraluminous infrared galaxies (ULIRGs; Sanders & Mirabel 1996). ULIRGs are sys-

tems of a major merger and harbor substantial quantities of infrared-emitting dust centrally concentrated within their nuclei (Sanders et al. 1988; Clements et al. 1996; Borne et al. 2000; Veilleux et al. 2002). Their powerful energy sources are energetic radiation from active galactic nuclei (AGNs) and starbursts (Genzel et al. 1998; Veilleux et al. 2009). Both phenomena are activated by the inflow of gas resulting from merger events,

with the former possessing the capacity to terminate the latter by expelling the gas (Hopkins et al. 2006, 2008). The role of AGNs during mergers remains a subject of contention, closely linked to understanding the history of star formation and the growth of supermassive black holes within the obscured galactic population during the early Universe (Lonsdale et al. 2006b; Pérez-Torres et al. 2021).

When AGN activities halt the preceding star formation (AGN feedback), outflows emanating from the central engine are inferred to play a crucial role (e.g., Silk & Rees 1998; Cano-Díaz et al. 2012; Cresci et al. 2015; Carniani et al. 2016; Hekatelyne et al. 2024), where non-thermal jets are also supposed to contribute to this phenomenon (e.g., Dugan et al. 2017; Nesvadba et al. 2017; Singha et al. 2023; Su et al. 2023). Despite its importance, many questions about radio emission from AGNs in ULIRGs still need to be answered. A well-established correlation, spanning up to five orders of magnitude, exists between far-infrared and radio emission from galaxies (e.g., Helou et al. 1985; Condon et al. 1991a,b; Appleton et al. 2004; Gim et al. 2019). The intense radio emission, deviating significantly from this correlation, is attributed to the influence of AGN activities (e.g., Yun et al. 2001; Calistro Rivera et al. 2017; Wang et al. 2024). However, recent studies have shown that radio excess can only collect the most radio-loud AGNs (e.g., Morić et al. 2010; Solarz et al. 2019). Investigating the individual AGN activity at radio wavelengths remains crucial, even for objects whose radio excess has not been detected (cf. U et al. 2012).

This work will focus on the nearby ULIRG IRAS F01004–2237, located at $z = 0.118$, with an infrared luminosity of $10^{12.2} L_{\odot}$ (Kim & Sanders 1998). The object is categorized as an old merger, displaying slight distortions similar to those observed in mergers but lacking direct indications of tidal tails at optical wavelengths (Veilleux et al. 2002). While this object does not exhibit a pronounced radio excess, aligning with the far-infrared-radio correlation, it has been classified as a type-2 Seyfert based on optical observations (Allen et al. 1991; Yuan et al. 2010; Rodríguez Zaurín et al. 2013). Furthermore, Hayashi et al. (2021) have reported extended radio emission on a 100-kpc scale whose morphology is reminiscent of radio galaxies. Recently, large-scale (~ 100 kpc) radio continuum emission has been detected in a select number of ULIRGs (e.g., Nandi et al. 2021; Kukreti et al. 2022), and the properties of such emission in merging systems are still less known. Observational studies of IRAS F01004–2237 will yield valuable insights into the role of AGN jets in ULIRGs. At this moment, Hayashi et al. (2021) have suggested

that no detection of extended X-ray emission (Voges et al. 1999; Teng et al. 2005) supports an AGN origin of the extended radio emission, not a radio mini-halo or a radio relic associated with galaxy clusters (Ferretti et al. 2012; van Weeren et al. 2019). However, because this argument is only circumstantial and eliminative, detecting a high-brightness radio emission from an AGN through high resolution observations at the milliarcsecond (mas) scale is necessary.

This paper presents the results of multi-frequency radio observations conducted using the Very Long Baseline Array (VLBA). The high resolution achieved by very long baseline interferometry (VLBI) offers valuable insights into the presence of an AGN core responsible for the extended radio emission in IRAS F01004–2237. While VLBI imaging observations of ULIRGs have been widely conducted, they have been confined to a limited number of objects. For instance, in Mrk 231, a lobe structure and a recently emanating jet due to AGN activities have been identified (Carilli et al. 1998; Taylor et al. 1999; Ulvestad et al. 1999a,b; Lonsdale et al. 2003; Reynolds et al. 2009, 2013, 2017, 2020; Wang et al. 2021). A young radio source, indicative of the possible emergence of a new quasar in the context of merging galaxies, has been reported for IRAS 00182–7112 (Norris et al. 2012). In contrast, VLBI observations have also revealed radio supernovae (RSNe) and supernova remnants (SNRs), providing evidence of starburst activities in objects like Arp 220 (Lonsdale et al. 1998; Smith et al. 1998; Rovilos et al. 2005; Lonsdale et al. 2006a; Parra et al. 2007; Batejat et al. 2011, 2012; Varenius et al. 2019) and IRAS 17208–0014 (Momjian et al. 2003, 2006). Furthermore, composites of both AGNs and starbursts have been identified in several objects, such as IRAS 23365+3604 (Romero-Cañizales et al. 2012) and Mrk 273 (Carilli & Taylor 2000; Bondi et al. 2005). The new VLBA observations for IRAS F01004–2237 presented in this paper are expected to provide new insights into the origin of radio emission in the nuclear region of ULIRGs.

In this research, we employed the standard cosmological model with cold dark matter and a cosmological constant, adopting $H_0 = 70 \text{ km s}^{-1} \text{ Mpc}^{-1}$, $\Omega_M = 0.3$, and $\Omega_{\Lambda} = 0.7$, supported by observational studies from the past decades (e.g., Planck Collaboration et al. 2020). Under this model, at a redshift of the source ($z = 0.118$), 1 mas corresponds to a scale of 2.132 pc, and the luminosity distance, D_L , is 549.7 Mpc. The paper defines a spectral index, α , as $S_{\nu} \propto \nu^{\alpha}$, where S_{ν} represents flux density at frequency, ν .

2. OBSERVATIONS

The VLBA observation targeting IRAS F01004–2237 was executed on 2022 May 6, operating under the project code BH237C. The observation comprised a 6-hour session involving all ten VLBA stations. Four 128-MHz frequency subbands were employed throughout the observation for both right and left circular polarizations. Simultaneous observations were conducted at the S and X bands. The S -band observation operated at a center frequency of 2.268 GHz (hereafter 2.3 GHz) with a bandwidth of 128 MHz. The X -band observation spanned center frequencies of 8.304, 8.432, and 8.560 GHz for each subband, with the central frequency being 8.432 GHz (hereafter 8.4 GHz) and a total bandwidth of 384 MHz. Data were sampled at the Nyquist rate with two bits per sample, resulting in a total data rate of 4 Gbit s⁻¹. Only the parallel polarization hands were processed on the DiFX correlator (Deller et al. 2011). Each 128-MHz subband was subdivided into 256 spectral channels to maintain wide-field imaging capabilities and deal with radio frequency interference.

The observations were conducted in phase-referencing mode. Scans lasting 3–4 minutes on IRAS F01004–2237 were interspersed with 2-minute scans on a calibrator, J0108–2157, positioned 1.3 degrees from IRAS F01004–2237 (R.A. = 01^h 08^m 19^s.854172 and DEC. = -21° 57′ 38.75544″). During the scans for the target, both the antennas and the correlator were aligned with the optical position of IRAS F01004–2237 (R.A. = 01^h 02^m 49^s.920 and DEC. = -22° 21′ 57.000″). The total integration time for the target amounted to 145 minutes. Table 1 provides a summary of the observations for IRAS F01004–2237.

3. DATA REDUCTION

The data reduction followed a standard procedure using the Astronomical Image Processing System (AIPS; Greisen 2003) software developed at the National Radio Astronomy Observatory (NRAO). All analyses were performed independently in the 2.3-GHz and 8.4-GHz bands. First, we flagged the data observed at an elevation angle of less than 15 degrees to avoid large residuals from atmospheric propagation. For the 8.4-GHz data, we also flagged the baselines with the Fort Davis station (FD), where some observational problems had been reported in the correlation processing. Following the digital sampler bias corrections with the task ACCOR, we performed an *a priori* amplitude calibration with the task APCAL using system noise temperature measurements throughout the observation and gains provided

by each station. Atmospheric opacity correction was not made in this step. Then, we corrected Earth orientation parameters and ionospheric dispersive delay on the 2.3-GHz and 8.4-GHz data using the tasks VLBAEOPS and VLBATECR, respectively. Subsequently, fringe fitting of calibrators was performed on the data integrated over each scan using the task FRING. For the 8.4-GHz data, delays between subbands were also solved by the task MBDLY. Finally, we applied bandpass correction using the task BPASS for amplitude and phase using a fringe finder, S5 0016+73. We confirmed that all calibrators were detected on all baselines at all frequencies, except for the baselines involving FD at 8.4 GHz. At each step for the 2.3-GHz data, we identified and flagged radio frequency interference in the time and frequency domains using the tasks RFLAG and SPLAG.

Imaging processes were conducted using the CLEAN algorithm through the difmap software (Shepherd 1997). First, we integrated the visibilities of the phase calibrator, J0108–2157, every 20 seconds. Then, iterations of CLEAN and phase-only self-calibration were run by gradually reducing the solution time interval to 120, 60, and 30 minutes. Subsequently, we also solved for amplitude time variation by gradually reducing the solution interval to 120, 60, and 30 minutes. At each step, we confirmed that the coherence of the gain solutions was maintained. As a result, J0108–2157 shows point-like structures and core-jet morphology elongated toward the west at 2.3 and 8.4 GHz, respectively. Its peak and integrated flux densities at 2.3 GHz are 151.5 mJy beam⁻¹ and 170.9 mJy, respectively, whereas at 8.4 GHz, they are 70.1 mJy beam⁻¹ and 87.4 mJy, respectively. To derive antenna-based gain corrections for the RR and LL visibilities separately (Aaron 1997), we applied the AIPS task CALIB for J0108–2157. These gain solutions and the delay and rate solutions obtained through the fringe fitting were transferred to the target using the AIPS task CLCAL.

To identify the target, whose location within the telescope’s field of view was unknown, we initially utilized the task tclean in the Common Astronomy Software Applications (CASA; McMullin et al. 2007) package, equipped with wide-field imaging mode and multiterm multi-frequency synthesis capabilities. This approach successfully detected the target at 8.4 GHz, positioned ~ 1 arcsecond from the phase center, but not at 2.3 GHz. After adjusting the phase center of the visibility data to the location of the detected radio source using the AIPS task UVFIX, we conducted the subsequent imaging process for the 8.4-GHz data using the difmap software. After integrating the visibilities every 30 seconds, we made several rounds of CLEAN and phase-only self-

Table 1. VLBA Observations Summary for IRAS F01004–2237.

Date	Integration Time (min)	Phase Calibrator	Band	Frequency (GHz)	Band Width (MHz)	Beam Size	
						FWHM (mas ²)	PA (deg)
2022 May 6	145	J0108–2157	<i>S</i>	2.268	128	7.01 × 2.27	−1.6
			<i>X</i>	8.432	384	1.75 × 0.59	0.1

NOTE—Simultaneous observations were conducted at both the *S*- and *X*-bands. Beam sizes are determined in the uniformly weighted images.

calibration by gradually reducing the solution time interval to 120 and 60 minutes. Thus, we obtained the final image of the target at 8.4 GHz. Throughout the observations at the 8.4-GHz band, the amplitude fluctuations estimated by self-calibration to the phase calibrator consistently aligned with the absolute flux density uncertainties of 5% for VLBA at 15 GHz (Homan et al. 2002), which has also been applied to 8.4-GHz data (e.g., Reynolds et al. 2020).

4. RESULTS

We detected a point source at R.A. = $01^{\text{h}} 02^{\text{m}} 49^{\text{s}}.9911330 \pm 0^{\text{s}}.0000014$ and DEC. = $-22^{\circ} 21' 57.27013 \pm 0.00042''$. See Appendix A for estimates of the position errors (0.19 and 0.42 mas in R.A. and DEC. directions, respectively). The peak flux density in the naturally weighted image at 8.4 GHz, which is optimized for sensitivity, exceeds the 10σ level of the thermal noise. The position of the target coincides with a continuum source detected at 239.4 GHz (Imanishi et al. 2019) and an X-ray point source observed by the Chandra X-ray Observatory (Teng et al. 2005). Therefore, the radio source is likely to be associated with these submillimeter and X-ray sources.

Figure 1 shows a uniformly weighted image of the target at 8.4 GHz after phase-only self-calibration. The thermal noise and peak flux density measured in the image are 73 and $603 \mu\text{Jy beam}^{-1}$, respectively. The Gaussian fit for the image performed using the AIPS task IMFIT yields a full-width half maximum (FWHM) of the source as $1.83 \pm 0.23 \times 0.604 \pm 0.076 \text{ mas}^2$ at a position angle (PA) of 177.6 ± 3.8 degrees on the image, which is similar to the beam size of the image. The IMFIT was unable to determine the deconvolved size. The only value obtained was that of the major axis, which was ~ 0.5 arcseconds. We estimated the flux density of the source by summing the CLEAN components within

the beam, yielding a value of $556 \mu\text{Jy}^1$. Based on these constraints, the brightness temperature of the source, T_{b} , can be calculated using the equation:

$$1.8 \times 10^9 (1+z) \left(\frac{S_{\nu}}{\text{mJy}} \right) \left(\frac{\nu}{\text{GHz}} \right)^{-2} \left(\frac{\phi}{\text{mas}} \right)^{-2}, \quad (1)$$

where ϕ represents the source size (cf. Ulvestad et al. 2005). Consequently, we obtained $T_{\text{b}} \sim 10^{7.2}$ K for the detected source. Nevertheless this value depends on the beam size of the observation. We also measured the intrinsic source size by directly fitting a Gaussian component to the visibilities using the task modelfit in the difmap software and estimated the intrinsic brightness temperature, T'_{b} . The best-fit model is a Gaussian component with the integrated flux density of $561 \mu\text{Jy}$ and deconvolved source size of $0.842 \times 0.168 \text{ mas}^2$ at a PA of -14.7 degrees², corresponding to the linear size of ~ 1 pc. As a result, we obtained $T'_{\text{b}} \sim 10^{8.1}$ K.

At 2.3 GHz, we obtained a thermal noise level of $159 \mu\text{Jy beam}^{-1}$ for a uniformly weighted image with a beam size of $7.01 \times 2.27 \text{ mas}^2$ at a PA of -1.6 degrees. We adopted 3σ as an upper limit of the flux density at the frequency. As a result, the spectral index between 2.3 and 8.4 GHz, $\alpha_{2.3}^{8.4}$, can be constrained as $\alpha_{2.3}^{8.4} > 0.12$. Figure 2 illustrates the radio spectrum of the source with measurements for the extended structure obtained from previous studies. Table 2 summarizes our measurements on the images.

¹ The difmap software computes the peak flux density by converting the flux density per pixel in the image into flux density per beam size. Consequently, the flux density value of an unresolved source, smaller than the beam size, can be less than its peak flux density value.

² The task modelfit in the difmap software does not output fitting errors.

Table 2. Flux measurement of IRAS F01004–2237

Band (GHz)	RMS ($\mu\text{Jy beam}^{-1}$)	Source Size on the Image		Peak flux density ($\mu\text{Jy beam}^{-1}$)	Integrated flux density (μJy)	Brightness Temperature (K)
		FWHM (mas^2)	PA (deg)			
2.3	159	< 473	< 473	< $10^{7.1}$
8.4	73	$1.83 \pm 0.23 \times 0.604 \pm 0.076$	177.6 ± 3.8	603 ± 79	556 ± 78	$10^{7.2}$

NOTE—All values are measured in the uniformly weighted images. The flux density error is determined by taking the root mean square (RMS) of the thermal noise and the systematic uncertainty of amplitude calibration, set at 5%.

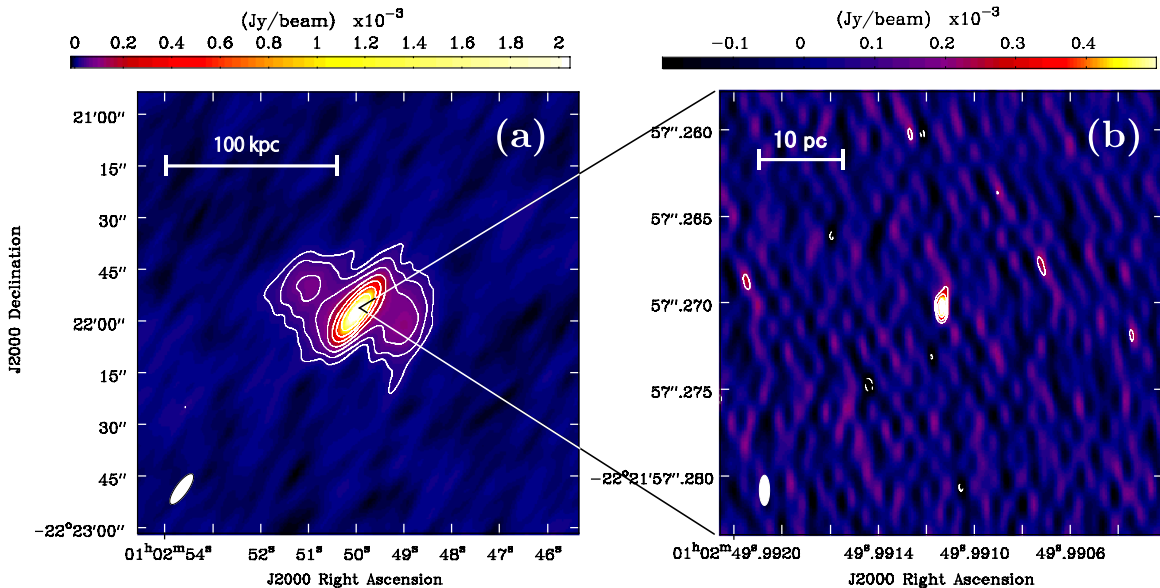


Figure 1. (a) A J2000 image at 9.0 GHz with a resolution of 13.0×4.7 arcsecond² at a PA of 143 degrees, presented in Hayashi et al. (2021). Contour levels commence at $17 \mu\text{Jy beam}^{-1}$, corresponding to the 3σ noise level of the image, and are subsequently multiplied by a factor of 2. The peak flux density in the image is $2.7 \text{ mJy beam}^{-1}$. For more details on imaging processes, please see the reference paper. (b) A uniformly weighted VLBA image at 8.4 GHz with a resolution of $1.75 \times 0.59 \text{ mas}^2$ at a PA of 0.1 degrees. Contour levels commence at $219 \mu\text{Jy beam}^{-1}$, corresponding to the 3σ noise level of the image, and are subsequently multiplied by a factor of $\sqrt{2}$. The peak flux density in the image is $603 \mu\text{Jy beam}^{-1}$.

5. DISCUSSION

5.1. Origin of the Radio Emission

The radio emission from the compact source in IRAS F01004–2237 has a high intrinsic brightness temperature of $T'_b \sim 10^{8.1}$ K, as measured by the VLBA observation at 8.4 GHz. This feature indicates the presence of non-thermal phenomena, such as an AGN, RSN, or SNR, because compact starbursts that lack these phenomena have $T'_b \lesssim 10^5$ K (Condon 1992). Additionally, the source size of ~ 1 pc rules out the possibility of a single RSN or SNR. The surface brightness and size of RSNe and SNRs typically exhibit a correlation, commonly known as the Σ - D relation (Clark & Caswell 1976; Huang & Thaddeus 1985). According to this em-

pirical relation, a 1-pc RSN or SNR has a surface brightness of $\sim 10^{-15} \text{ W m}^{-2} \text{ Hz}^{-1} \text{ str}^{-1}$ (e.g., Urošević et al. 2005; Bandiera & Petruk 2010), which corresponds to $T'_b \sim 10^6$ K. Although the presence of multiple compact and young SNRs/RSNe densely packed in the small area of ~ 1 pc might account for the observational results, such a scenario is deemed highly improbable considering the typical separation between RSNe/SNRs of ~ 10 pc in the nucleus of Arp 220 (e.g., Lonsdale et al. 2006a). Therefore, achieving $T'_b \sim 10^{8.1}$ K is only possible through AGN activity. This active radio source is a candidate for the AGN core that powers the 100-kpc extended radio emission reported by Hayashi et al. (2021).

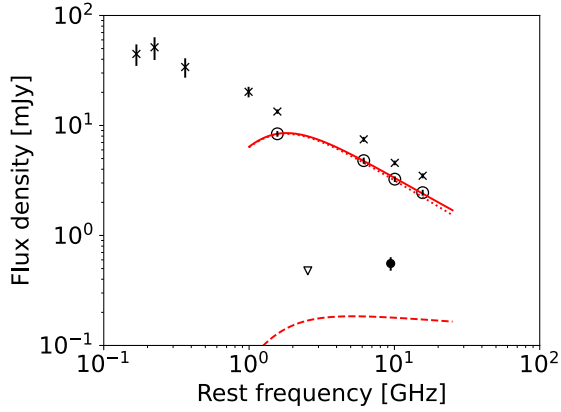


Figure 2. Radio spectrum of IRAS F01004–2237. Crosses denote the integrated flux density of the source as provided by TGSS at 150 MHz (Intema et al. 2017), GLEAM survey at 200 MHz (Hurley-Walker et al. 2017), WISH at 352 MHz (De Breuck et al. 2002), RACS at 887.5 MHz (Hale et al. 2021), and VLA observations by Hayashi et al. (2021). Open circles represent the core flux density reported by Hayashi et al. (2021). A filled circle and an open triangle depict the flux density at 8.4 GHz and its 3σ upper limit at 2.3 GHz, respectively, obtained through VLBA observations in this study. A red solid line illustrates the model for the VLA core as reported in Hayashi et al. (2021), assuming a non-thermal component (dotted line) absorbed by ambient thermal plasma with free-free emission (dashed line).

IRAS F01004–2237 exhibits a far-infrared to radio ratio of $q = 2.49 \pm 0.04$ computed from the far-infrared flux density and the radio flux density at 1.4 GHz (Hayashi et al. 2021), which aligns with the average value of 2.34 observed for entire galaxies (Yun et al. 2001). While low q values, indicative of high radio power, are typically attributed to an AGN activity, IRAS F01004–2237, which hosts the AGN, does not exhibit such a characteristic. Recent studies have revealed the presence of AGNs even in objects with moderate q values (e.g., Morić et al. 2010; Solarz et al. 2019), with IRAS F01004–2237 serving as an example of such an object.

Caution should be exercised when estimating star formation rates for these sources. According to the relation derived by Panuzzo et al. (2003), a star formation rate is calculated as $258.4 \times 10^{-30} L_{8.4} M_{\odot} \text{yr}^{-1}$, where $L_{8.4}$ represents a specific radio luminosity at 8.4 GHz in units of $\text{erg s}^{-1} \text{Hz}^{-1}$ (Clemens et al. 2010). For IRAS F01004–2237, the star formation rate is obtained as $\sim 300 M_{\odot} \text{yr}^{-1}$ in the core region of the JVLA image (Figure 1a; Hayashi et al. 2021), assuming that all radio emission is associated with star formation (e.g., Clemens et al. 2010). However, we have found that AGN activity contributes to the radio emission of IRAS F01004–2237. Therefore, at least the flux contribution from the compact radio source must be subtracted, resulting in a star

formation rate of $\lesssim 250 M_{\odot} \text{yr}^{-1}$. If the emission not detected by the VLBA observations is also of AGN origin, this constraint may even be an overestimate.

5.2. Physical Constraints of the Active Radio Source

The compact radio source originating from an AGN activity exhibits a spectral index of $\alpha_{2,3}^{8.4} > 0.12$, suggesting the potential influence of Synchrotron self-absorption (SSA) and/or free-free absorption (FFA). Below, we discuss the possibility of each absorption mechanism in explaining the observed outcomes.

The magnetic field strength responsible for SSA, B_{SSA} , is determined by

$$\left(\frac{B_{\text{SSA}}}{\text{mG}}\right) = 3.1 \times 10^4 \left(\frac{\nu_p}{\text{GHz}}\right)^5 \left(\frac{S_p}{\text{mJy}}\right)^{-2} \left(\frac{\phi}{\text{mas}}\right)^4 (1+z)^{-1}, \quad (2)$$

where S_p is the peak flux density observed at frequency, ν_p (Kellermann & Pauliny-Toth 1981). To relate S_p to the observed flux density at 8.4 GHz, we assume the spectral indices of the optically thin and thick parts to be $\alpha = -0.7$ and 2.5, respectively. On a different aspect, employing minimum energy conditions, where the energy densities of electrons and magnetic fields are roughly equal, we can compute the equipartition magnetic field strength, B_{eq} , as

$$\left(\frac{B_{\text{eq}}}{\text{mG}}\right) = 2.9 \times 10^{-11} \left(\frac{R}{\text{pc}}\right)^{-\frac{6}{7}} \left(\frac{L}{\text{erg/s}}\right)^{\frac{2}{7}} (1+k)^{\frac{2}{7}} \quad (3)$$

where R , L , and k represent the radius of the component, bolometric luminosity, and energy ratio between heavy particles and electrons (Pacholczyk 1970). We assume $k = 1$, but it is worth noting that B_{eq} remains relatively insensitive to the specific values of k . We approximate $L \simeq 4\pi D_L^2 S_p \nu_p$ for the bolometric luminosity (e.g., Feng et al. 2006). Figure 3 represents the physical conditions constrained by Equations (2) and (3) for specific values of ν_p .

Assuming that SSA is a consequence of an equipartition magnetic field, i.e., $B_{\text{SSA}} = B_{\text{eq}}$, and the spectral peak is present at a few GHz, we derive a magnetic field strength on an order of 100 mG and a source size of an order of 0.01 pc (see Figure 3). Although these values reasonably align with expectations for the base of the jet (cf. Ro et al. 2023), we have obtained the deconvolved source size of an order of 1 pc, which is inconsistent with the estimation assuming SSA. Therefore, SSA alone is not capable of explaining the physical condition of the active radio source.

On the other hand, FFA can alternatively contribute to the observed spectrum of the active radio source. The

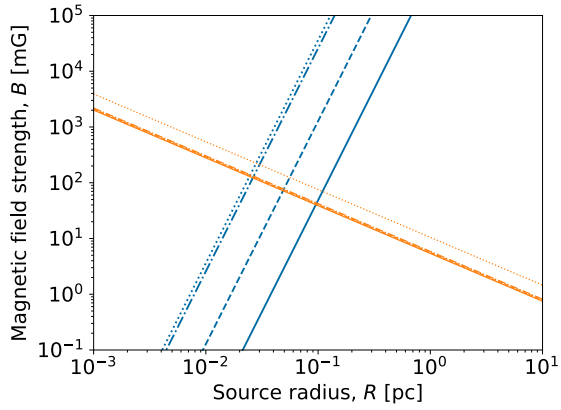


Figure 3. Physical conditions of the non-thermal plasma under the assumptions of SSA and equipartition. The plot demonstrates the relationship between plasma radius, R , and magnetic field strength, B . The blue lines represent constraints imposed by SSA (Equation 2), while the orange lines indicate constraints under the equipartition condition (Equation 3). The solid, dashed, dash-dotted, and dotted lines of each color correspond to peak frequencies at rest, ν_p , of 3, 5, 8, and 15 GHz, respectively. The equipartition condition given in Equation 3 is insensitive to luminosity, resulting in the overlapping of the orange solid line with the dashed and dot-dashed lines.

substantial presence of ambient plasma associated with the host galaxy plays a significant role in enhancing the optical depth of FFA. We can calculate the optical depth of FFA, τ_ν , as

$$\tau_\nu = 0.46 \left(\frac{r}{\text{pc}} \right) \left(\frac{T_e}{\text{K}} \right)^{-\frac{3}{2}} \left(\frac{n_e}{\text{cm}^{-3}} \right)^2 \left(\frac{\nu}{\text{GHz}} \right)^{-2.1} \epsilon, \quad (4)$$

where r , T_e , n_e , and ϵ represent the thermal plasma's radius, electron temperature, electron density, and volume filling factor, respectively (e.g., [Kameno 2001](#)). The spectrum peaks at the frequency where $\tau_\nu \sim 1$ is satisfied. Figure 4 depicts the physical condition of the plasma constrained by Equation (4), assuming $T_e = 10^4$ K and certain values of ν_p . At the same time, the thermal plasma, which gives rise to FFA, radiates free-free emission (FFE). In an optically thin regime, we can derive the electron density of the thermal plasma producing FFE as

$$\left(\frac{n_e}{\text{cm}^{-3}} \right) = 3.6 \times 10^3 \left(\frac{r}{\text{pc}} \right)^{-\frac{3}{2}} \left(\frac{T_e}{\text{K}} \right)^{\frac{1}{4}} \left(\frac{S_{\text{ff}}}{\text{Jy}} \right)^{\frac{1}{2}} \left(\frac{D_L}{\text{Mpc}} \right)^{-1/2}, \quad (5)$$

where S_{ff} is the flux density at an optically thin regime (e.g., [Harper-Clark & Murray 2009](#)). FFE contributes an order of 0.1 mJy to IRAS F01004–2237 in an optically thin regime ([Imanishi et al. 2019](#); [Hayashi et al. 2021](#), see Figure 2). Figure 4 also illustrates the physical

parameters constrained based on the conditions imposed by the FFE and assuming certain values of S_{ff} .

Assuming the spectral peak is present at a few GHz, we estimate r and $n_e \epsilon^{1/2}$ to be an order of 100 pc and 100 cm^{-3} , respectively (see Figure 4). These estimates are consistent with the conditions found in local ULIRGs, whose typical size of thermal plasma exhibiting FFE is ~ 1 kpc ([Barcos-Muñoz et al. 2017](#)), and typical electron densities are $\sim 100 \text{ cm}^{-3}$ determined through optical emission-line ratios ([Veilleux et al. 1999](#)). Therefore, FFA resulting from thermal plasma within the merging system can be a primary cause of the flat or inverted radio spectrum observed in the active radio source.

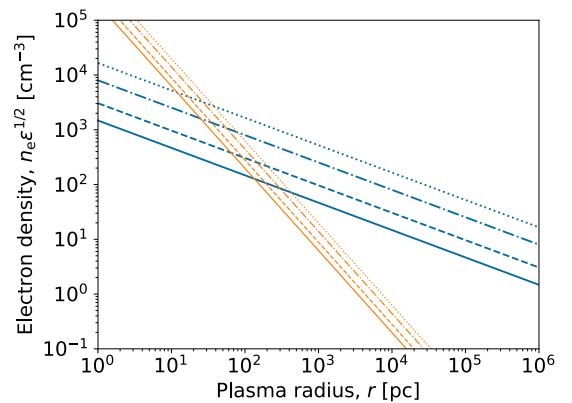


Figure 4. Physical conditions of the ambient thermal plasma assuming an electron temperature of 10^4 K. The plot demonstrates the relationship between the plasma radius, r , and electron density considering the filling factor, $n_e \epsilon^{1/2}$. The blue lines represent constraints imposed by FFA (Equation 4), with the solid, dashed, dash-dotted, and dotted lines corresponding to peak frequencies at rest, ν_p , of 1, 2, 5, and 10 GHz, respectively. The orange lines indicate the constraints imposed by FFE (Equation 5), with the solid, dashed, dash-dotted, and dotted lines corresponding to flux density at optically thin regime due to FFE of 0.1, 0.2, 0.5, and 1.0 mJy, respectively.

5.3. Multiwavelength Characteristics and Evolutionary Implications of the AGN

IRAS F01004–2237 has an optical counterpart located encompassing the compact radio source, which is classified as a type-2 Seyfert AGN ([Yuan et al. 2010](#); [Rodríguez Zaurín et al. 2013](#)) and hosts a supermassive black hole with a mass of $2.5 \times 10^7 M_\odot$ ([Dasyra et al. 2006](#)). This AGN is currently active, marked by an increase of luminosity and spectral change in optical and infrared wavelengths attributed to tidal disruption events, whereby stars undergo gravitational disruption as they closely approach the supermassive black holes

(Dou et al. 2017; Tadhunter et al. 2017, 2021). At X-ray, a point source has been identified at the coordinates of R.A. = $01^{\text{h}} 02^{\text{m}} 49^{\text{s}}.99$, DEC. = $-22^{\circ} 21' 57.3''$ obtained through the Chandra X-ray Observatory (Teng et al. 2005) using the Advanced CCD Imaging Spectrometer (ACIS)³. The position of the compact radio source aligns with the X-ray source, whose spectrum is very soft and lacks direct AGN emission below 10 keV, suggesting a Compton-thick circumnuclear environment (Nardini & Risaliti 2011). This argument is consistent with the infrared spectra of IRAS F01004–2237, which show signs of AGN obscuration (Imanishi et al. 2007, 2008; Veilleux et al. 2009; Nardini et al. 2010).

Despite the optical luminosity of the source not meeting the criteria, the host galaxy of IRAS F01004–2237 possesses a nearly stellar radial profile similar to that of quasars lacking tidal tails or loops (Surace et al. 1998), indicating an old merger (Veilleux et al. 2002). Hayashi et al. (2021) have mentioned that the absence of extended X-ray features (Voges et al. 1999; Teng et al. 2005) hints at the potential AGN origin of the 100-kpc scale radio emission. Moreover, this object exhibits an HCN-to-HCO⁺ ($J = 3-2$) flux-density ratio higher than unity in the northwest-southeast direction within its central few 100 pc (Imanishi et al. 2019), where mechanical heating attributed to an AGN jet is one considerable explanation (cf. Aalto et al. 2012; Izumi et al. 2013; Hagiwara et al. 2024). Therefore, we can infer that this object is a ULIRG that was once shrouded by dust and actively forming stars but is presently undergoing a process of dust dispersion due to AGN activities, including those of jets (cf. Su et al. 2023).

5.4. Contribution of the Jet Activities to AGN Feedback

In the following analysis, we explore whether the jet power of IRAS 01004–2237 contribute to AGN feedback. Under the minimum energy condition (cf. Equation 3), the time-averaged kinetic power of AGN jets fueling the extended features in a radio galaxy is derived as

$$\left(\frac{P_{\text{jet}}}{\text{erg/s}}\right) = 3 \times 10^{15} \left(\frac{L_{151}}{\text{erg/s/Hz/sr}}\right)^{\frac{6}{7}} f^{\frac{3}{2}}, \quad (6)$$

where L_{151} ($= S_{151} D_L^2$) represents the specific radio luminosity at 151 MHz calculated from the flux density at 151 MHz, S_{151} , and f denotes a parameter accounting for systematic error in the model assumptions (Willott

et al. 1999). This relationship applies regardless of the radio power of jet activities (Godfrey & Shabala 2013). Taking the flux density of 44.7 ± 9.9 mJy provided by the TIFR GMRT Sky Survey (TGSS; Intema et al. 2017) at 150 MHz as S_{151} , the specific radio luminosity of IRAS F01004–2237 is $L_{151} = (1.27 \pm 0.28) \times 10^{30} \text{ erg s}^{-1} \text{ Hz}^{-1} \text{ sr}^{-1}$. In this luminosity range, a value of $f = 20$ (i.e., low radiative efficiency) can be applied (Godfrey & Shabala 2013). Substituting these values to Equation (6), we obtain $P_{\text{jet}} \sim 2 \times 10^{43} \text{ erg s}^{-1}$. Note that the spatial resolution of TGSS (~ 25 arcseconds) is insufficient to separate the core from the extended structure as in Figure 1, resulting in the measured flux density also including contributions from star formation. Therefore, the kinetic power of the jets estimated here represents an upper bound.

On another front, in IRAS F01004–2237, a blueshifted broad component with a FWHM $\sim 1400 \text{ km s}^{-1}$ and a velocity shift of $\sim -800 \text{ km s}^{-1}$ in the [O III] emission line have been documented (Rodríguez Zaurín et al. 2013). Additionally, prominent blueshifted emission wings have been observed in the Ly α and N V profiles (Martin et al. 2015), and a distinct P-Cygni profile has been detected in the OH doublet at $119 \mu\text{m}$ (Spoon et al. 2013), solidifying the presence of a thermal wind in this object. Spence et al. (2018) estimated its kinetic energy to be an order of $\sim 10^{41-42} \text{ erg s}^{-1}$ based on the [O III] emission line. Moreover, an O VI broad absorption line (BAL) is evident in IRAS F01004–2237, with a lower limit of its kinetic energy determined to be $10^{40.6} \text{ erg s}^{-1}$ (Liu et al. 2022). Relative to the total AGN radiative power, which is $(8.8 \pm 0.4) \times 10^{44} \text{ erg s}^{-1}$ estimated from the [O III] emission line, the contribution of the thermal outflow to the AGN feedback has been considered to be modest (Spence et al. 2018).

Although there is considerable uncertainty in estimating the transfer efficiencies of kinetic energies (e.g., Wagner et al. 2012; Nesvadba et al. 2017), the kinetic power of the jet in IRAS F01004–2237, P_{jet} , can surpass that of the thermal outflow and may possess sufficient potency to disperse the surrounding medium (cf. Nyland et al. 2013). Consequently, this ULIRG could be in a transition phase to become a quasar, accompanied by jet activity, as in the case observed in IRAS 00182–7112 (Spoon et al. 2007, 2009; Norris et al. 2012). Further validation of this hypothesis will require the detection of jet emission at radio frequencies linking the pc-scale active radio source to the extended structure at the 100-kpc scale (cf. Pérez-Torres et al. 2010; Su et al. 2023). If this connection is confirmed, the involvement of jet activities in ULIRGs would emerge as a significant factor in galaxy evolution triggered by merger events.

³ The reference paper does not provide a position error, which would typically be on the order of 0.1 arcseconds. This estimate is based on the assumption that the ACIS observations with 1-arcsecond spatial resolution detect a signal greater than 5σ .

6. SUMMARY

Our VLBA imaging of the ULIRG IRAS F01004–2237 has identified the pc-scale compact radio source with an intrinsic brightness temperature of $T'_b \sim 10^{8.1}$ K at 8.4 GHz and a spectral index of $\alpha_{2.3}^{8.4} > 0.12$. These characteristics indicate the presence of non-thermal phenomena, which cannot be attributed to a typical RSN or SNR, suggesting an AGN origin. While the connection between the pc-scale and 100-kpc structures of the source still remains ambiguous, the identified active radio source is an AGN core potentially driving the extended features. An investigation of the physical conditions has revealed that FFA primarily contributes to the observed radio spectrum. Also from a multi-wavelength perspective, the AGN in IRAS F01004–2237 is obscured in a dense environment. The kinetic power of the jet, estimated from the 100-kpc extended features, can be greater than that of the thermal outflow, which could blow away the surrounding medium and contribute to AGN feedback during galaxy evolution.

This research has used the VizieR catalogue access tool, CDS, Strasbourg, France. Additionally, we utilized the NASA/IPAC Extragalactic Database (NED), operated by the Jet Propulsion Laboratory, California Institute of Technology, under contract with the National Aeronautics and Space Administration. Cosmological calculations are conducted using a calculator provided by Wright (2006). The NRAO operating VLBA is a facility of the National Science Foundation operated under a cooperative agreement by Associated Universities, Inc. This work used the Swinburne University of Technology software correlator (Deller et al. 2011), developed as part of the Australian Major National Research Facilities Programme and operated under license.

Facilities: VLBA (NRAO)

Software: AIPS (Greisen 2003), astropy (Astropy Collaboration et al. 2013, 2018) CASA (McMullin et al. 2007), difmap (Shepherd 1997).

APPENDIX

A. POSITIONAL ACCURACY OF THE COMPACT RADIO SOURCE IN IRAS F01004–2237

The position error of the compact radio source at 8.4 GHz detected in IRAS F01004–2237 (0.19 and 0.42 mas in R.A. and DEC. directions, respectively) was estimated by the root-sum-square of the individual astrometric error contributions (e.g., Pradel et al. 2006; Hada et al. 2011). Table 3 summarizes the estimated error budget in our phase-referencing observations. The positional accuracy of the phase calibrator was obtained from the Radio Fundamental Catalog⁴. The flux peak accuracy for the target and calibrator was calculated by dividing the beam size by the signal-to-noise ratio of the uniformly weighted images. We estimated that the residual errors arising from propagation delays due to the non-dispersive tropospheric medium (e.g., Reid et al. 1999) and the dispersive ionospheric medium (e.g., Lestrade et al. 1990) by assuming a zenith angle of 65 degrees and a zenith angle difference between the target and calibrator to be 1 degree. Based on the typical zenith delay used in the model for the VLBA correlator, we adopted a non-dispersive residual of 3 cm (Risaliti et al. 1999). The total electron content of the dispersive ionospheric medium was $\sim 2 \times 10^{17} \text{ m}^{-2}$ over the sky of the VLBA stations, which was obtained from the US Total Electron Content Product Archive⁵ maintained by the National Oceanic and Atmospheric Administration. The global ionospheric model based on GPS satellites has an accuracy of about 10–25% (Mannucci et al. 1998). Conservatively, we adopted the uncertainty of 25%, corresponding to $\sim 5 \times 10^{16} \text{ m}^{-2}$. The contributions due to Earth orientation parameters and antenna positions were estimated based on the simulation presented in Pradel et al. (2006).

REFERENCES

- Aalto, S., Garcia-Burillo, S., Muller, S., et al. 2012, *A&A*, 537, A44, doi: [10.1051/0004-6361/201117919](https://doi.org/10.1051/0004-6361/201117919)
- Aaron, S. E. 1997, EVN Document No. 78
- Allen, D. A., Norris, R. P., Meadows, V. S., & Roche, P. F. 1991, *MNRAS*, 248, 528, doi: [10.1093/mnras/248.3.528](https://doi.org/10.1093/mnras/248.3.528)
- Appleton, P. N., Fadda, D. T., Marleau, F. R., et al. 2004, *ApJS*, 154, 147, doi: [10.1086/422425](https://doi.org/10.1086/422425)
- ⁴ <http://astrogeo.org/sol/rfc/rfc.2023d/>
- ⁵ <https://www.ngdc.noaa.gov/stp/iono/ustec/index.html>

Table 3. Error budget for the 8.4-GHz VLBA observation for IRAS F01004–2237 (in μas).

Error component	R.A.	DEC.
Source coordinates (calibrator)	170	340
Flux peak accuracy (calibrator)	2	5
Flux peak accuracy (target)	72	210
Tropospheric residuals	45	126
Ionospheric residuals	5	14
Antenna position	2	8
Earth orientation	1	8
Total	190	419

- Astropy Collaboration, Robitaille, T. P., Tollerud, E. J., et al. 2013, *A&A*, 558, A33, doi: [10.1051/0004-6361/201322068](https://doi.org/10.1051/0004-6361/201322068)
- Astropy Collaboration, Price-Whelan, A. M., Sipőcz, B. M., et al. 2018, *AJ*, 156, 123, doi: [10.3847/1538-3881/aabc4f](https://doi.org/10.3847/1538-3881/aabc4f)
- Bandiera, R., & Petruk, O. 2010, *A&A*, 509, A34, doi: [10.1051/0004-6361/200912244](https://doi.org/10.1051/0004-6361/200912244)
- Barcos-Muñoz, L., Leroy, A. K., Evans, A. S., et al. 2017, *ApJ*, 843, 117, doi: [10.3847/1538-4357/aa789a](https://doi.org/10.3847/1538-4357/aa789a)
- Batejat, F., Conway, J. E., Hurley, R., et al. 2011, *ApJ*, 740, 95, doi: [10.1088/0004-637X/740/2/95](https://doi.org/10.1088/0004-637X/740/2/95)
- Batejat, F., Conway, J. E., Rushton, A., et al. 2012, *A&A*, 542, L24, doi: [10.1051/0004-6361/201219235](https://doi.org/10.1051/0004-6361/201219235)
- Bondi, M., Pérez-Torres, M. A., Dallacasa, D., & Muxlow, T. W. B. 2005, *MNRAS*, 361, 748, doi: [10.1111/j.1365-2966.2005.09206.x](https://doi.org/10.1111/j.1365-2966.2005.09206.x)
- Borne, K. D., Bushouse, H., Lucas, R. A., & Colina, L. 2000, *ApJL*, 529, L77, doi: [10.1086/312461](https://doi.org/10.1086/312461)
- Calistro Rivera, G., Williams, W. L., Hardcastle, M. J., et al. 2017, *MNRAS*, 469, 3468, doi: [10.1093/mnras/stx1040](https://doi.org/10.1093/mnras/stx1040)
- Cano-Díaz, M., Maiolino, R., Marconi, A., et al. 2012, *A&A*, 537, L8, doi: [10.1051/0004-6361/201118358](https://doi.org/10.1051/0004-6361/201118358)
- Carilli, C. L., & Taylor, G. B. 2000, *ApJL*, 532, L95, doi: [10.1086/312584](https://doi.org/10.1086/312584)
- Carilli, C. L., Wrobel, J. M., & Ulvestad, J. S. 1998, *AJ*, 115, 928, doi: [10.1086/300253](https://doi.org/10.1086/300253)
- Carniani, S., Marconi, A., Maiolino, R., et al. 2016, *A&A*, 591, A28, doi: [10.1051/0004-6361/201528037](https://doi.org/10.1051/0004-6361/201528037)
- Clark, D. H., & Caswell, J. L. 1976, *MNRAS*, 174, 267, doi: [10.1093/mnras/174.2.267](https://doi.org/10.1093/mnras/174.2.267)
- Clemens, M. S., Scaife, A., Vega, O., & Bressan, A. 2010, *MNRAS*, 405, 887, doi: [10.1111/j.1365-2966.2010.16534.x](https://doi.org/10.1111/j.1365-2966.2010.16534.x)
- Clements, D. L., Sutherland, W. J., McMahon, R. G., & Saunders, W. 1996, *MNRAS*, 279, 477, doi: [10.1093/mnras/279.2.477](https://doi.org/10.1093/mnras/279.2.477)
- Condon, J. J. 1992, *ARA&A*, 30, 575, doi: [10.1146/annurev.aa.30.090192.003043](https://doi.org/10.1146/annurev.aa.30.090192.003043)
- Condon, J. J., Anderson, M. L., & Helou, G. 1991a, *ApJ*, 376, 95, doi: [10.1086/170258](https://doi.org/10.1086/170258)
- Condon, J. J., Huang, Z. P., Yin, Q. F., & Thuan, T. X. 1991b, *ApJ*, 378, 65, doi: [10.1086/170407](https://doi.org/10.1086/170407)
- Cresci, G., Mainieri, V., Brusa, M., et al. 2015, *ApJ*, 799, 82, doi: [10.1088/0004-637X/799/1/82](https://doi.org/10.1088/0004-637X/799/1/82)
- Dasyra, K. M., Tacconi, L. J., Davies, R. I., et al. 2006, *ApJ*, 651, 835, doi: [10.1086/507834](https://doi.org/10.1086/507834)
- De Breuck, C., Tang, Y., de Bruyn, A. G., Röttgering, H., & van Breugel, W. 2002, *A&A*, 394, 59, doi: [10.1051/0004-6361:20021115](https://doi.org/10.1051/0004-6361:20021115)
- Deller, A. T., Brisken, W. F., Phillips, C. J., et al. 2011, *PASP*, 123, 275, doi: [10.1086/658907](https://doi.org/10.1086/658907)
- Dou, L., Wang, T., Yan, L., et al. 2017, *ApJL*, 841, L8, doi: [10.3847/2041-8213/aa7130](https://doi.org/10.3847/2041-8213/aa7130)
- Dugan, Z., Gaibler, V., & Silk, J. 2017, *ApJ*, 844, 37, doi: [10.3847/1538-4357/aa7566](https://doi.org/10.3847/1538-4357/aa7566)
- Feng, S. W., Shen, Z. Q., Cai, H. B., et al. 2006, *A&A*, 456, 97, doi: [10.1051/0004-6361:20054678](https://doi.org/10.1051/0004-6361:20054678)
- Feretti, L., Giovannini, G., Govoni, F., & Murgia, M. 2012, *A&A Rv*, 20, 54, doi: [10.1007/s00159-012-0054-z](https://doi.org/10.1007/s00159-012-0054-z)
- Genzel, R., Lutz, D., Sturm, E., et al. 1998, *ApJ*, 498, 579, doi: [10.1086/305576](https://doi.org/10.1086/305576)
- Gim, H. B., Yun, M. S., Owen, F. N., et al. 2019, *ApJ*, 875, 80, doi: [10.3847/1538-4357/ab1011](https://doi.org/10.3847/1538-4357/ab1011)
- Godfrey, L. E. H., & Shabala, S. S. 2013, *ApJ*, 767, 12, doi: [10.1088/0004-637X/767/1/12](https://doi.org/10.1088/0004-637X/767/1/12)
- Greisen, E. W. 2003, *Information Handling in Astronomy - Historical Vistas*, 285, 109
- Hada, K., Doi, A., Kino, M., et al. 2011, *Nature*, 477, 185, doi: [10.1038/nature10387](https://doi.org/10.1038/nature10387)
- Hagiwara, Y., Baan, W. A., Imanishi, M., & Diamond, P. 2024, *MNRAS*, 528, 3668, doi: [10.1093/mnras/stae075](https://doi.org/10.1093/mnras/stae075)

- Hale, C. L., McConnell, D., Thomson, A. J. M., et al. 2021, *PASA*, 38, e058, doi: [10.1017/pasa.2021.47](https://doi.org/10.1017/pasa.2021.47)
- Harper-Clark, E., & Murray, N. 2009, *ApJ*, 693, 1696, doi: [10.1088/0004-637X/693/2/1696](https://doi.org/10.1088/0004-637X/693/2/1696)
- Hayashi, T. J., Hagiwara, Y., & Imanishi, M. 2021, *MNRAS*, 504, 2675, doi: [10.1093/mnras/stab1084](https://doi.org/10.1093/mnras/stab1084)
- Hekatelyne, C., Storchi-Bergmann, T., Riffel, R. A., et al. 2024, *MNRAS*, 527, 10844, doi: [10.1093/mnras/stad3963](https://doi.org/10.1093/mnras/stad3963)
- Helou, G., Soifer, B. T., & Rowan-Robinson, M. 1985, *ApJL*, 298, L7, doi: [10.1086/184556](https://doi.org/10.1086/184556)
- Homan, D. C., Ojha, R., Wardle, J. F. C., et al. 2002, *ApJ*, 568, 99, doi: [10.1086/338701](https://doi.org/10.1086/338701)
- Hopkins, P. F., Hernquist, L., Cox, T. J., et al. 2006, *ApJS*, 163, 1, doi: [10.1086/499298](https://doi.org/10.1086/499298)
- Hopkins, P. F., Hernquist, L., Cox, T. J., & Kereš, D. 2008, *ApJS*, 175, 356, doi: [10.1086/524362](https://doi.org/10.1086/524362)
- Huang, Y. L., & Thaddeus, P. 1985, *ApJL*, 295, L13, doi: [10.1086/184528](https://doi.org/10.1086/184528)
- Hurley-Walker, N., Callingham, J. R., Hancock, P. J., et al. 2017, *MNRAS*, 464, 1146, doi: [10.1093/mnras/stw2337](https://doi.org/10.1093/mnras/stw2337)
- Imanishi, M., Dudley, C. C., Maiolino, R., et al. 2007, *ApJS*, 171, 72, doi: [10.1086/513715](https://doi.org/10.1086/513715)
- Imanishi, M., Nakagawa, T., Ohyama, Y., et al. 2008, *PASJ*, 60, 489. <https://arxiv.org/abs/0808.0363>
- Imanishi, M., Nakanishi, K., & Izumi, T. 2019, *ApJS*, 241, 19, doi: [10.3847/1538-4365/ab05b9](https://doi.org/10.3847/1538-4365/ab05b9)
- Intema, H. T., Jagannathan, P., Mooley, K. P., & Frail, D. A. 2017, *A&A*, 598, A78, doi: [10.1051/0004-6361/201628536](https://doi.org/10.1051/0004-6361/201628536)
- Izumi, T., Kohno, K., Martín, S., et al. 2013, *PASJ*, 65, 100, doi: [10.1093/pasj/65.5.100](https://doi.org/10.1093/pasj/65.5.100)
- Kameno, S. 2001, PhD thesis, The University of Tokyo
- Kellermann, K. I., & Pauliny-Toth, I. I. K. 1981, *ARA&A*, 19, 373, doi: [10.1146/annurev.aa.19.090181.002105](https://doi.org/10.1146/annurev.aa.19.090181.002105)
- Kim, D. C., & Sanders, D. B. 1998, *ApJS*, 119, 41, doi: [10.1086/313148](https://doi.org/10.1086/313148)
- Kukreti, P., Morganti, R., Bondi, M., et al. 2022, *A&A*, 664, A25, doi: [10.1051/0004-6361/202243174](https://doi.org/10.1051/0004-6361/202243174)
- Lestrade, J. F., Rogers, A. E. E., Whitney, A. R., et al. 1990, *AJ*, 99, 1663, doi: [10.1086/115447](https://doi.org/10.1086/115447)
- Liu, W., Veilleux, S., Rupke, D. S. N., et al. 2022, *ApJ*, 934, 160, doi: [10.3847/1538-4357/ac7a46](https://doi.org/10.3847/1538-4357/ac7a46)
- Lonsdale, C. J., Diamond, P. J., Thrall, H., Smith, H. E., & Lonsdale, C. J. 2006a, *ApJ*, 647, 185, doi: [10.1086/505193](https://doi.org/10.1086/505193)
- Lonsdale, C. J., Farrah, D., & Smith, H. E. 2006b, in *Astrophysics Update 2*, ed. J. W. Mason, 285, doi: [10.1007/3-540-30313-8_9](https://doi.org/10.1007/3-540-30313-8_9)
- Lonsdale, C. J., Lonsdale, C. J., Diamond, P. J., & Smith, H. E. 1998, *ApJL*, 493, L13, doi: [10.1086/311121](https://doi.org/10.1086/311121)
- Lonsdale, C. J., Lonsdale, C. J., Smith, H. E., & Diamond, P. J. 2003, *ApJ*, 592, 804, doi: [10.1086/375778](https://doi.org/10.1086/375778)
- Mannucci, A. J., Wilson, B. D., Yuan, D. N., et al. 1998, *Radio Science*, 33, 565, doi: [10.1029/97RS02707](https://doi.org/10.1029/97RS02707)
- Martin, C. L., Dijkstra, M., Henry, A., et al. 2015, *ApJ*, 803, 6, doi: [10.1088/0004-637X/803/1/6](https://doi.org/10.1088/0004-637X/803/1/6)
- McMullin, J. P., Waters, B., Schiebel, D., Young, W., & Golap, K. 2007, in *Astronomical Society of the Pacific Conference Series*, Vol. 376, *Astronomical Data Analysis Software and Systems XVI*, ed. R. A. Shaw, F. Hill, & D. J. Bell, 127
- Momjian, E., Romney, J. D., Carilli, C. L., & Troland, T. H. 2006, *ApJ*, 653, 1172, doi: [10.1086/508699](https://doi.org/10.1086/508699)
- Momjian, E., Romney, J. D., Carilli, C. L., Troland, T. H., & Taylor, G. B. 2003, *ApJ*, 587, 160, doi: [10.1086/367722](https://doi.org/10.1086/367722)
- Morić, I., Smolčić, V., Kimball, A., et al. 2010, *ApJ*, 724, 779, doi: [10.1088/0004-637X/724/1/779](https://doi.org/10.1088/0004-637X/724/1/779)
- Nandi, S., Das, M., & Dwarakanath, K. S. 2021, *MNRAS*, 503, 5746, doi: [10.1093/mnras/stab275](https://doi.org/10.1093/mnras/stab275)
- Nardini, E., & Risaliti, G. 2011, *MNRAS*, 415, 619, doi: [10.1111/j.1365-2966.2011.18732.x](https://doi.org/10.1111/j.1365-2966.2011.18732.x)
- Nardini, E., Risaliti, G., Watabe, Y., Salvati, M., & Sani, E. 2010, *MNRAS*, 405, 2505, doi: [10.1111/j.1365-2966.2010.16618.x](https://doi.org/10.1111/j.1365-2966.2010.16618.x)
- Nesvadba, N. P. H., De Breuck, C., Lehnert, M. D., Best, P. N., & Collet, C. 2017, *A&A*, 599, A123, doi: [10.1051/0004-6361/201528040](https://doi.org/10.1051/0004-6361/201528040)
- Norris, R. P., Lenc, E., Roy, A. L., & Spoon, H. 2012, *MNRAS*, 422, 1453, doi: [10.1111/j.1365-2966.2012.20717.x](https://doi.org/10.1111/j.1365-2966.2012.20717.x)
- Nyland, K., Alatalo, K., Wrobel, J. M., et al. 2013, *ApJ*, 779, 173, doi: [10.1088/0004-637X/779/2/173](https://doi.org/10.1088/0004-637X/779/2/173)
- Pacholczyk, A. G. 1970, *Radio astrophysics. Nonthermal processes in galactic and extragalactic sources*
- Panuzzo, P., Bressan, A., Granato, G. L., Silva, L., & Danese, L. 2003, *A&A*, 409, 99, doi: [10.1051/0004-6361:20031094](https://doi.org/10.1051/0004-6361:20031094)
- Parra, R., Conway, J. E., Diamond, P. J., et al. 2007, *ApJ*, 659, 314, doi: [10.1086/511813](https://doi.org/10.1086/511813)
- Pérez-Torres, M., Mattila, S., Alonso-Herrero, A., Aalto, S., & Efstathiou, A. 2021, *A&A Rv*, 29, 2, doi: [10.1007/s00159-020-00128-x](https://doi.org/10.1007/s00159-020-00128-x)
- Pérez-Torres, M. A., Alberdi, A., Romero-Cañizales, C., & Bondi, M. 2010, *A&A*, 519, L5, doi: [10.1051/0004-6361/201015462](https://doi.org/10.1051/0004-6361/201015462)
- Planck Collaboration, Aghanim, N., Akrami, Y., et al. 2020, *A&A*, 641, A6, doi: [10.1051/0004-6361/201833910](https://doi.org/10.1051/0004-6361/201833910)
- Pradel, N., Charlot, P., & Lestrade, J. F. 2006, *A&A*, 452, 1099, doi: [10.1051/0004-6361:20053021](https://doi.org/10.1051/0004-6361:20053021)

- Reid, M. J., Readhead, A. C. S., Vermeulen, R. C., & Treuhaft, R. N. 1999, *ApJ*, 524, 816, doi: [10.1086/307855](https://doi.org/10.1086/307855)
- Reynolds, C., Punsly, B., Kharb, P., O’Dea, C. P., & Wrobel, J. 2009, *ApJ*, 706, 851, doi: [10.1088/0004-637X/706/1/851](https://doi.org/10.1088/0004-637X/706/1/851)
- Reynolds, C., Punsly, B., Miniutti, G., O’Dea, C. P., & Hurley-Walker, N. 2017, *ApJ*, 836, 155, doi: [10.3847/1538-4357/836/2/155](https://doi.org/10.3847/1538-4357/836/2/155)
- . 2020, *ApJ*, 891, 59, doi: [10.3847/1538-4357/ab72f0](https://doi.org/10.3847/1538-4357/ab72f0)
- Reynolds, C., Punsly, B., O’Dea, C. P., & Hurley-Walker, N. 2013, *ApJL*, 776, L21, doi: [10.1088/2041-8205/776/2/L21](https://doi.org/10.1088/2041-8205/776/2/L21)
- Risaliti, G., Maiolino, R., & Salvati, M. 1999, *ApJ*, 522, 157, doi: [10.1086/307623](https://doi.org/10.1086/307623)
- Ro, H., Kino, M., Sohn, B. W., et al. 2023, *A&A*, 673, A159, doi: [10.1051/0004-6361/202142988](https://doi.org/10.1051/0004-6361/202142988)
- Rodríguez Zaurín, J., Tadhunter, C. N., Rose, M., & Holt, J. 2013, *MNRAS*, 432, 138, doi: [10.1093/mnras/stt423](https://doi.org/10.1093/mnras/stt423)
- Romero-Cañizales, C., Pérez-Torres, M. Á., & Alberdi, A. 2012, *MNRAS*, 422, 510, doi: [10.1111/j.1365-2966.2012.20627.x](https://doi.org/10.1111/j.1365-2966.2012.20627.x)
- Rovilos, E., Diamond, P. J., Lonsdale, C. J., Smith, H. E., & Lonsdale, C. J. 2005, *MNRAS*, 359, 827, doi: [10.1111/j.1365-2966.2005.08853.x](https://doi.org/10.1111/j.1365-2966.2005.08853.x)
- Sanders, D. B., & Mirabel, I. F. 1996, *ARA&A*, 34, 749, doi: [10.1146/annurev.astro.34.1.749](https://doi.org/10.1146/annurev.astro.34.1.749)
- Sanders, D. B., Soifer, B. T., Elias, J. H., et al. 1988, *ApJ*, 325, 74, doi: [10.1086/165983](https://doi.org/10.1086/165983)
- Shepherd, M. C. 1997, in *Astronomical Society of the Pacific Conference Series*, Vol. 125, *Astronomical Data Analysis Software and Systems VI*, ed. G. Hunt & H. Payne, 77–+
- Silk, J., & Rees, M. J. 1998, *A&A*, 331, L1, doi: [10.48550/arXiv.astro-ph/9801013](https://doi.org/10.48550/arXiv.astro-ph/9801013)
- Singha, M., Winkel, N., Vaddi, S., et al. 2023, *ApJ*, 959, 107, doi: [10.3847/1538-4357/ad004d](https://doi.org/10.3847/1538-4357/ad004d)
- Smith, H. E., Lonsdale, C. J., Lonsdale, C. J., & Diamond, P. J. 1998, *ApJL*, 493, L17, doi: [10.1086/311122](https://doi.org/10.1086/311122)
- Solarz, A., Pollo, A., Bilicki, M., et al. 2019, *PASJ*, 71, 28, doi: [10.1093/pasj/psz013](https://doi.org/10.1093/pasj/psz013)
- Spence, R. A. W., Tadhunter, C. N., Rose, M., & Rodríguez Zaurín, J. 2018, *MNRAS*, 478, 2438, doi: [10.1093/mnras/sty1046](https://doi.org/10.1093/mnras/sty1046)
- Spoon, H. W. W., Armus, L., Marshall, J. A., et al. 2009, *ApJ*, 693, 1223, doi: [10.1088/0004-637X/693/2/1223](https://doi.org/10.1088/0004-637X/693/2/1223)
- Spoon, H. W. W., Marshall, J. A., Houck, J. R., et al. 2007, *ApJL*, 654, L49, doi: [10.1086/511268](https://doi.org/10.1086/511268)
- Spoon, H. W. W., Farrah, D., Lebouteiller, V., et al. 2013, *ApJ*, 775, 127, doi: [10.1088/0004-637X/775/2/127](https://doi.org/10.1088/0004-637X/775/2/127)
- Su, R., Mahony, E. K., Gu, M., et al. 2023, *MNRAS*, 520, 5712, doi: [10.1093/mnras/stad370](https://doi.org/10.1093/mnras/stad370)
- Surace, J. A., Sanders, D. B., Vacca, W. D., Veilleux, S., & Mazzarella, J. M. 1998, *ApJ*, 492, 116, doi: [10.1086/305028](https://doi.org/10.1086/305028)
- Tadhunter, C., Patel, M., & Mullaney, J. 2021, *MNRAS*, 504, 4377, doi: [10.1093/mnras/stab1105](https://doi.org/10.1093/mnras/stab1105)
- Tadhunter, C., Spence, R., Rose, M., Mullaney, J., & Crowther, P. 2017, *Nature Astronomy*, 1, 0061, doi: [10.1038/s41550-017-0061](https://doi.org/10.1038/s41550-017-0061)
- Taylor, G. B., Silver, C. S., Ulvestad, J. S., & Carilli, C. L. 1999, *ApJ*, 519, 185, doi: [10.1086/307362](https://doi.org/10.1086/307362)
- Teng, S. H., Wilson, A. S., Veilleux, S., et al. 2005, *ApJ*, 633, 664, doi: [10.1086/491595](https://doi.org/10.1086/491595)
- U, V., Sanders, D. B., Mazzarella, J. M., et al. 2012, *ApJS*, 203, 9, doi: [10.1088/0067-0049/203/1/9](https://doi.org/10.1088/0067-0049/203/1/9)
- Ulvestad, J. S., Antonucci, R. R. J., & Barvainis, R. 2005, *ApJ*, 621, 123, doi: [10.1086/427426](https://doi.org/10.1086/427426)
- Ulvestad, J. S., Wrobel, J. M., & Carilli, C. L. 1999a, *ApJ*, 516, 127, doi: [10.1086/307111](https://doi.org/10.1086/307111)
- Ulvestad, J. S., Wrobel, J. M., Roy, A. L., et al. 1999b, *ApJL*, 517, L81, doi: [10.1086/312040](https://doi.org/10.1086/312040)
- Urošević, D., Pannuti, T. G., Duric, N., & Theodorou, A. 2005, *A&A*, 435, 437, doi: [10.1051/0004-6361:20042535](https://doi.org/10.1051/0004-6361:20042535)
- van Weeren, R. J., de Gasperin, F., Akamatsu, H., et al. 2019, *SSRv*, 215, 16, doi: [10.1007/s11214-019-0584-z](https://doi.org/10.1007/s11214-019-0584-z)
- Varenius, E., Conway, J. E., Batejat, F., et al. 2019, *A&A*, 623, A173, doi: [10.1051/0004-6361/201730631](https://doi.org/10.1051/0004-6361/201730631)
- Veilleux, S., Kim, D. C., & Sanders, D. B. 1999, *ApJ*, 522, 113, doi: [10.1086/307634](https://doi.org/10.1086/307634)
- . 2002, *ApJS*, 143, 315, doi: [10.1086/343844](https://doi.org/10.1086/343844)
- Veilleux, S., Rupke, D. S. N., Kim, D. C., et al. 2009, *ApJS*, 182, 628, doi: [10.1088/0067-0049/182/2/628](https://doi.org/10.1088/0067-0049/182/2/628)
- Voges, W., Aschenbach, B., Boller, T., et al. 1999, *A&A*, 349, 389. <https://arxiv.org/abs/astro-ph/9909315>
- Wagner, A. Y., Bicknell, G. V., & Umemura, M. 2012, *ApJ*, 757, 136, doi: [10.1088/0004-637X/757/2/136](https://doi.org/10.1088/0004-637X/757/2/136)
- Wang, A., An, T., Jaiswal, S., et al. 2021, *MNRAS*, 504, 3823, doi: [10.1093/mnras/stab587](https://doi.org/10.1093/mnras/stab587)
- Wang, Y., Wang, T., Liu, D., et al. 2024, *arXiv e-prints*, arXiv:2401.04924, doi: [10.48550/arXiv.2401.04924](https://doi.org/10.48550/arXiv.2401.04924)
- Willott, C. J., Rawlings, S., Blundell, K. M., & Lacy, M. 1999, *MNRAS*, 309, 1017, doi: [10.1046/j.1365-8711.1999.02907.x](https://doi.org/10.1046/j.1365-8711.1999.02907.x)
- Wright, E. L. 2006, *PASP*, 118, 1711, doi: [10.1086/510102](https://doi.org/10.1086/510102)
- Yuan, T. T., Kewley, L. J., & Sanders, D. B. 2010, *ApJ*, 709, 884, doi: [10.1088/0004-637X/709/2/884](https://doi.org/10.1088/0004-637X/709/2/884)
- Yun, M. S., Reddy, N. A., & Condon, J. J. 2001, *ApJ*, 554, 803, doi: [10.1086/323145](https://doi.org/10.1086/323145)